Fermilab

FERMILAB-FN-693 July 2000

Beam Loss, Collimation and Shielding at the Fermilab Proton Driver*

A. I. Drozhdin, O. E. Krivosheev and N. V. Mokhov

Fermi National Accelerator Laboratory

P.O. Box 500, Batavia, Illinois 60510

July 5, 2000

Abstract

Summary of studies is presented towards minimization of beam loss in the 16 GeV Fermilab Proton Driver for a preliminary lattice design. Tolerable beam loss is deduced based on MARS-calculated radiation fields and on regulatory limits for prompt radiation, hands-on maintenance, ground-water activation and component lifetime. A proposed *3-stage collimation system* designed through detailed Monte-Carlo simulations allows for localization of more than 99% of beam loss in a special 60 m long utility section. Beam loss in the rest of the machine is on average only 0.2 W/m. Possible use of a bent crystal as a primary collimator is explored. Based on the calculated source term and radiation attenuation around the tunnel, the shielding parameters are derived both for the arcs and for the 'hot' utility section. It is shown that despite of challenging parameters of the proposed machine, beam loss and induced radiation effects can be reduced to the allowable levels.

*Work supported by the U. S. Department of Energy under contract No. DE-AC02-76CH03000

1 Introduction

The Proton Driver under design at Fermilab is a 16 GeV high intensity rapid cycling proton synchrotron [1, 2]. The lattice parameters [2, 3] used in this paper are presented in Table 1. The machine's function is to deliver intense short proton bunches to the target for muon production to serve a neutrino factory and—as a second stage—a muon collider, to replace the Fermilab Booster and to allow for a new physics program with intense beams. A very high beam power of $\sim$1.2 MW (4 MW at a second stage) implies serious constrains on beam losses in the machine [4]. As will be shown below, the main concern are the hands-on maintenance and ground-water activation. Only with a very efficient beam collimation system [5] can one reduce uncontrolled beam losses in the machine to allowable level. Massive local shielding is needed around the collimators. The entire complex must be well shielded to allow a non-controlled access to the outside surfaces under normal operation and accidental beam loss.

Table 1: Proton Driver parameters.

Injection kinetic energy (GeV)	0.4
Top kinetic energy (GeV)	16
Circumference (m)	647.9
Injected 95% emittance ε_N (mm.mrad)	3
After painting emittance ε_N (mm.mrad)	60
27 turn painting injection duration (μs)	90
Protons per bunch at injection	8.25×10^{12}
Protons per bunch at extraction	7.5×10^{12}
Number of bunches	4
Total intensity at injection	3.3×10^{13}
Total intensity at extraction	3×10^{13}
Repetition rate (Hz)	15

In this study, a multi-turn particle tracking in the lattice with halo proton interactions with the collimators is done with the STRUCT [6] code. Protons lost on the machine components are stored to the files for the next step of calculations with the MARS [7, 8] code. Full-scale Monte Carlo hadronic and electromagnetic shower simulations in the lattice elements, shielding, tunnel and surrounding dirt with realistic geometry, materials and magnetic field are done with MARS14. This paper summarizes the results on the tolerable beam loss, on the proposed beam collimation system and on the required radiation shielding at the 16-GeV Proton Driver for a preliminary lattice design. Although the final lattice can be different, a majority of the results and main conclusions of this paper should remain valid.

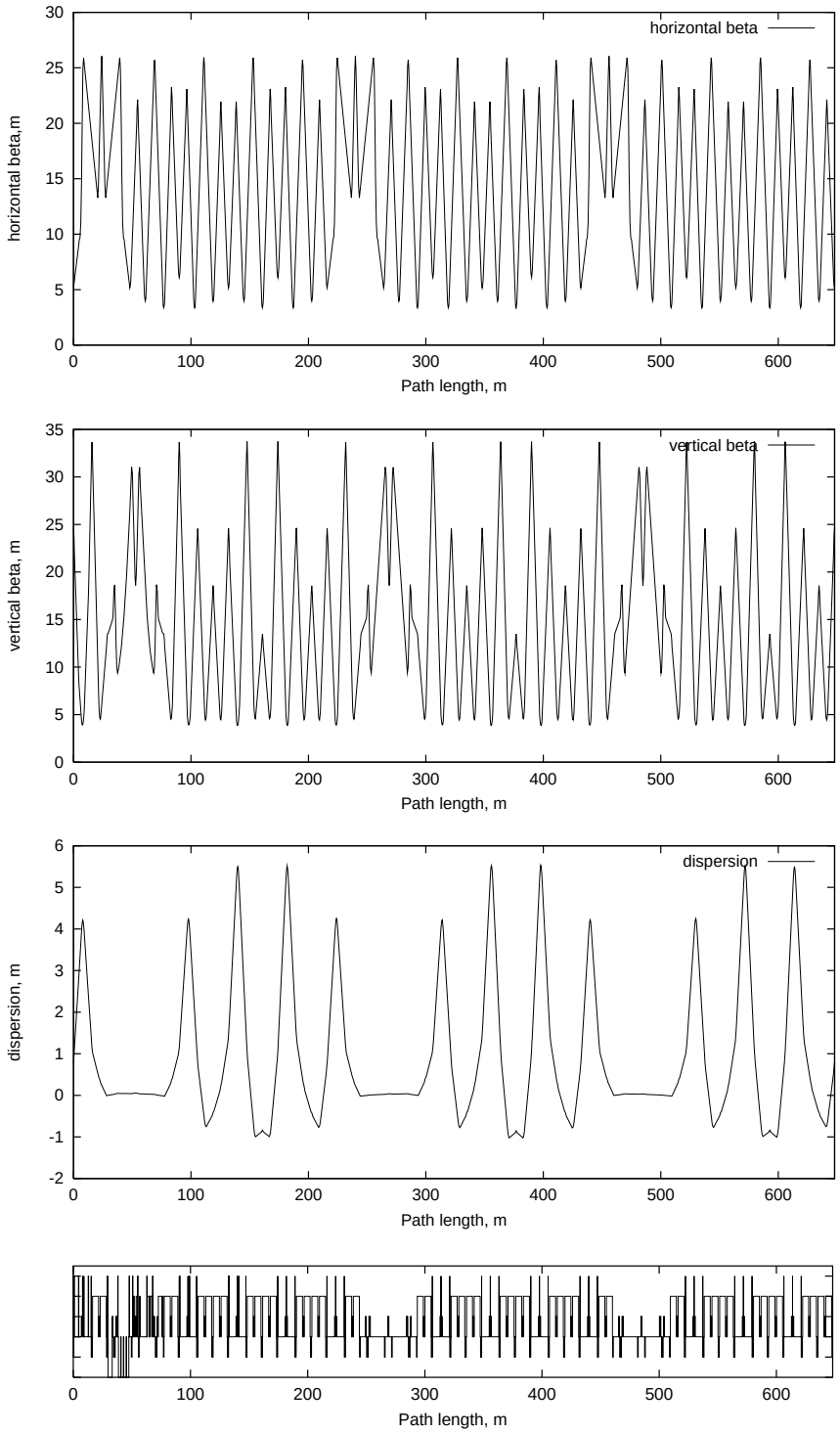

Figure 1: Proton Driver beta functions and dispersion.

2 Proton Driver

There are three 48 meter long straight sections in the considered preliminary lattice. One of them and its two preceding cells (60 m total) are called together *utility section*. It is used for the beam injection, extraction and collimation, and two others are used for the RF cavities. The Proton Driver beta functions and dispersion along the arcs and utility section are shown in Figs. 1 and 2. The beam extraction system is located in the first part of the utility section. It consists of a 3.5-m vertical kicker magnet and three Lambertson magnets (Lamb-1, 2, 3) which extract the beam in the horizontal plane (Fig. 2). A painting injection system [9] located in the second part of the utility section (Fig. 2) is required to provide an uniform beam density distribution in the transverse plane to reduce a space-charge effect at injection. It is done by using two sets of horizontal and vertical fast kicker-magnets.

3 Tolerable Beam Loss

3.1 Regulatory Limits

1. Prompt radiation in non-controlled areas on accessible outside surfaces of the shield: 0.25 mrem/hr at normal operation and 5 mrem/hr for the worst case catastrophic accident. An often used definition of a beam accident as a loss of the full beam at a single point for an hour requires further clarification for the machine of such a class.

2. Hands-on maintenance: residual dose rate of 100 mrem/hr at 30 cm from the component surface, after 100 day irradiation at 4 hrs after shutdown. Averaged over the components dose rate should be less than 10-20 mrem/hr. It is worth to note that the (100 days / 4 hrs / 30 cm) condition is practically equivalent to the (30 days / 1 day / 0 cm) one.

3. Ground-water activation: do not exceed radionuclide concentration limits $C_{i,reg}$ of 20 pCi/ml for ^{3}H and 0.4 pCi/ml for ^{22}Na.

4. Component radiation damage: machine component lifetime of 20 years. Assume 10 Mrad/yr in the hot spots.

3.2 Ground-Water Activation

Fermilab Radiological Control Manual defines concentration limits for the two most dangerous isotopes: ^{3}H (half time 12.32 y, β^{-}) and ^{22}Na (half time 2.604 y, β^{+} and γ). Respective concentration limits $C_{i,reg}$=20 pCi/ml and $C_{i,reg}$=0.4 pCi/ml correspond to 4 mrem/yr dose from drinking water. One should calculate creation and build-up of these nuclides. After irradiation over the time t, the concentration is

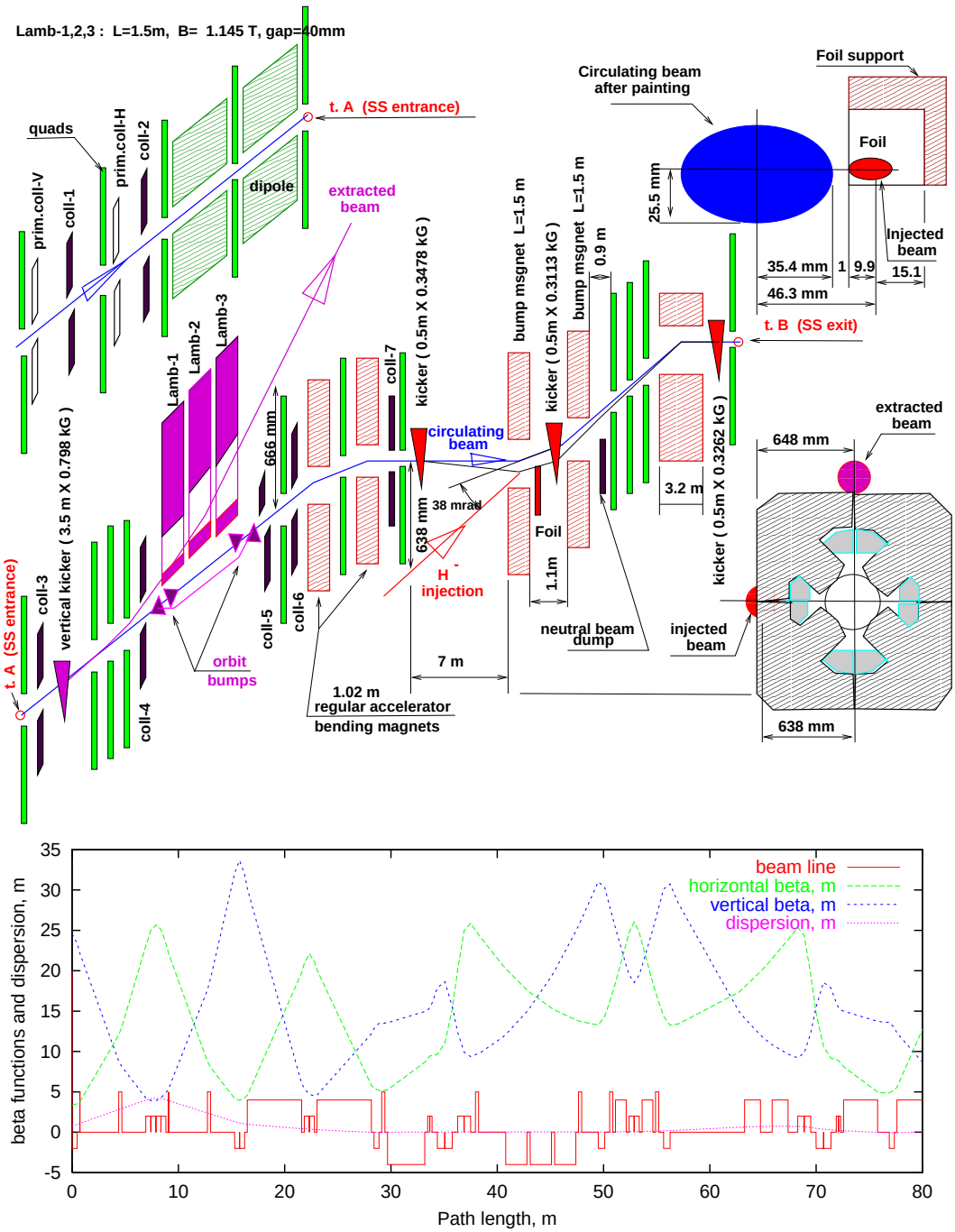

Figure 2: Beam extraction, collimation and beam painting schemes (top) and beta functions and dispersion in the utility section (bottom).

$$C_i(\frac{pCi}{ml \cdot y}) = \frac{1}{0.037} N_p S_{av} \frac{K_i L_i (1 - e^{-t/\tau})}{\rho_s w_i}, \quad (1)$$

where N_p is a number of protons per second, S_{av} is an average star density, K_i is a radionuclide production probability per star, L_i is a leachability factor, ρ_s is the soil density and w_i is a weight factor, i.e. the weight of water divided by the weight of soil needed to leach out 90 % of the leachable radioactivity, and τ_i is a mean lifetime of the radionuclide.

The $K_i L_i$ and w_i are site specific parameters. According to [10], $K_{[^3H]}$ $L_{[^3H]}$ is equal to $7.6 \cdot 10^{-3}$, $K_{[^{22}Na]}$ $L_{[^{22}Na]}$ is equal to $1.2 \cdot 10^{-4}$, and w_i are 0.325 and 0.66, respectively.

If there is more than one isotope created in the water mixture, the following condition must be fulfilled:

$$C_{tot} = \sum_{i=1}^{N} \frac{C_i}{C_{i,reg}} \leq 1, \quad (2)$$

where $C_{i,reg}$ are the above regulatory limits.

3.3 MARS Simulations and Radiation in Arcs

In this study, realistic MARS14 simulations are done in the arcs as:

- Full 3-D calculations of beam loss and showers induced in a 84-m arc cell.
- Detailed lattice description with dipoles, quadrupoles and unshielded beam pipes (see Figs. 3 and 4).
- 16 GeV beam losses are uniform longitudinally grazing at 1 mrad inward.
- Results are normalized per 1 W/m beam loss rate, that corresponds to 3.9×10^8 p/(m $\cdot$ sec).
- Round 2-m radius tunnel with a 0.4-m concrete wall followed by wet dirt.
- Accumulated dose, residual dose rate, ground-water activation and dose attenuation in dirt are calculated.

Fig. 5 shows calculated isocontours of neutron and charged hadron flux as well as energy deposition and residual dose in and around the arc components for the 16-GeV proton beam lost uniformly along the arc pipe. One sees pronounced peaks around the long bare beam pipes, which would drive the radiation environment in and near the beam-line. Corresponding peak residual dose rates on contact after 30 days of irradiation at 1 W/m uniform beam loss rate and 1 day of cooling are shown in Fig. 6. Remember that the above conditions give numerically the results

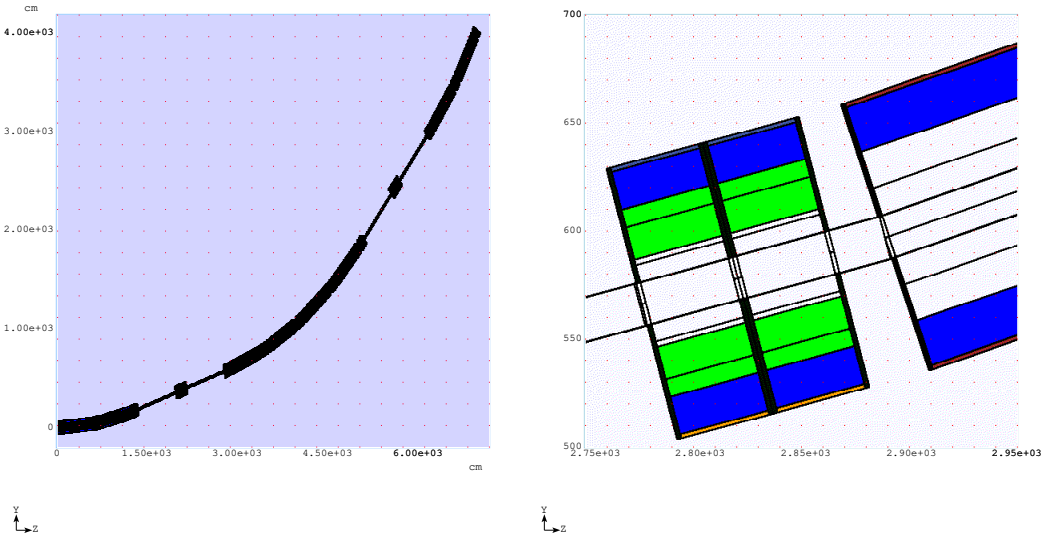

Figure 3: MARS model of a Proton Driver arc cell.

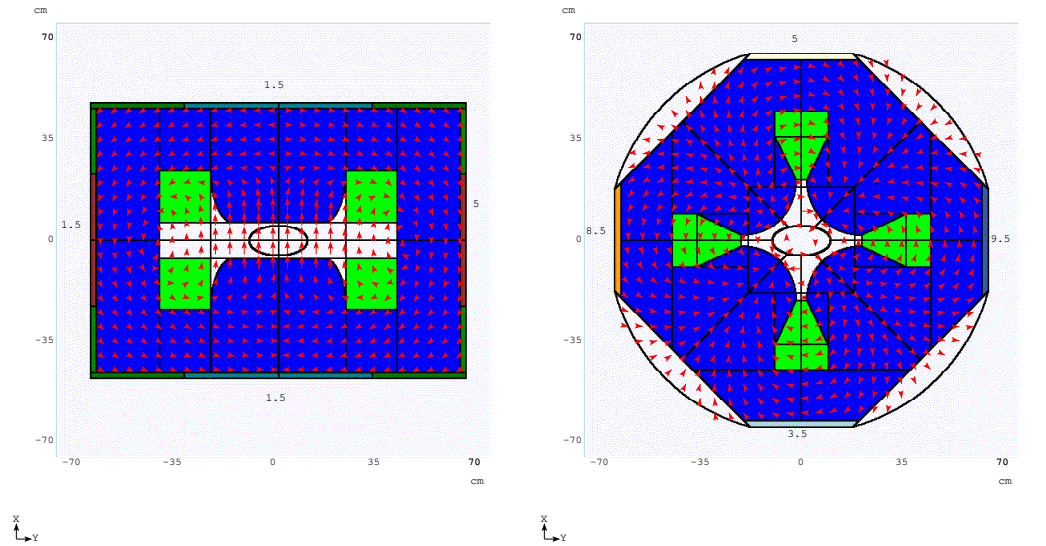

Figure 4: MARS model of arc dipole (left) and quadrupole (right).

very close to 100 day irradiation and 4 hours cooling for the dose at 30 cm radial distance from the component surface. The dose near the bare beam pipes exceeds the design goal for hot regions of 100 mrem/hr, being noticeably lower near the magnets due to significant absorption of soft photons in the dipole and quadrupole materials.

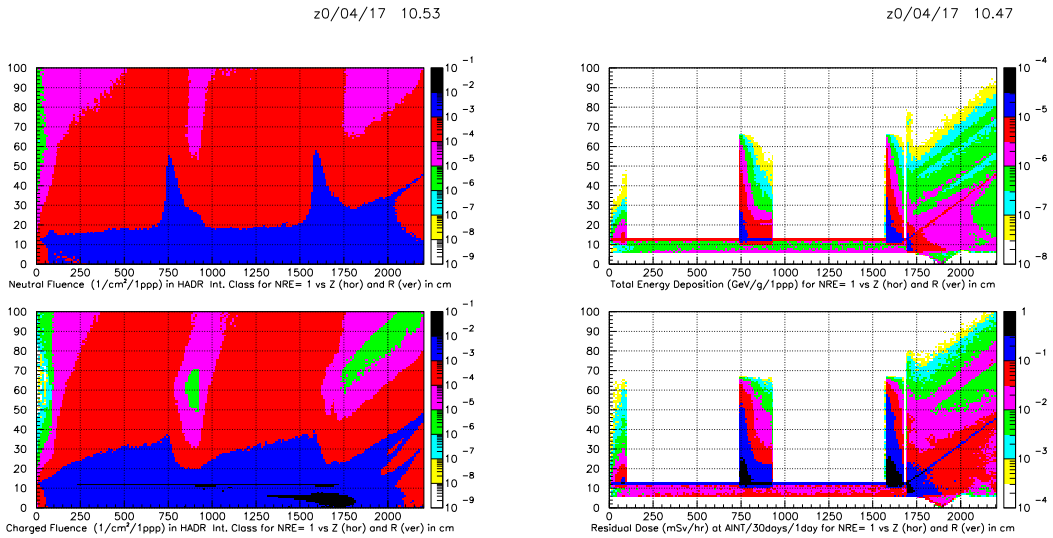

Figure 5: Neutron and charged hadron (E>20 MeV) flux (left) and energy deposition and residual dose rate (right).

3.4 Deduction of Allowable Beam Loss

Maximum residual dose rates calculated for the arc elements at 1 W/m uniform beam loss are shown in the third column of Table 3.4 along with the peak dose accumulated in the coils and with the parameter C_{tot} calculated according to Eq. (2). The last column gives corresponding beam loss rates calculated to meet the regulatory limits of Section 3.1: P_γ=100 mrem/hr, D=10 Mrad/yr and C_{tot}=1.

Table 2: Peak residual dose rate P_γ on 16 GeV lattice elements, accumulated dose D in dipole and quadrupole coils, ground-water activation parameter C_{tot} and allowable beam loss rate.

Value	Element	Peak at 1 W/m	Allowable loss (W/m)
P_γ (mrem/hr)	Long pipe	400	0.25
	Quad side	9.4	10.6
	Quad flange	34	2.94
	Dipole side	5	20
	Dipole flange	20	5
D (Mrad/yr)	Coil	2	5
C_{tot}	Ground water	1.5	0.6

To meet a non-migrating ground-water limit immediately outside the 40-cm tunnel wall, the beam loss rate should be below 0.6 W/m. With local shielding of open drifts (probably needed anyway) or thicker walls or dirt insulation, ground-water can

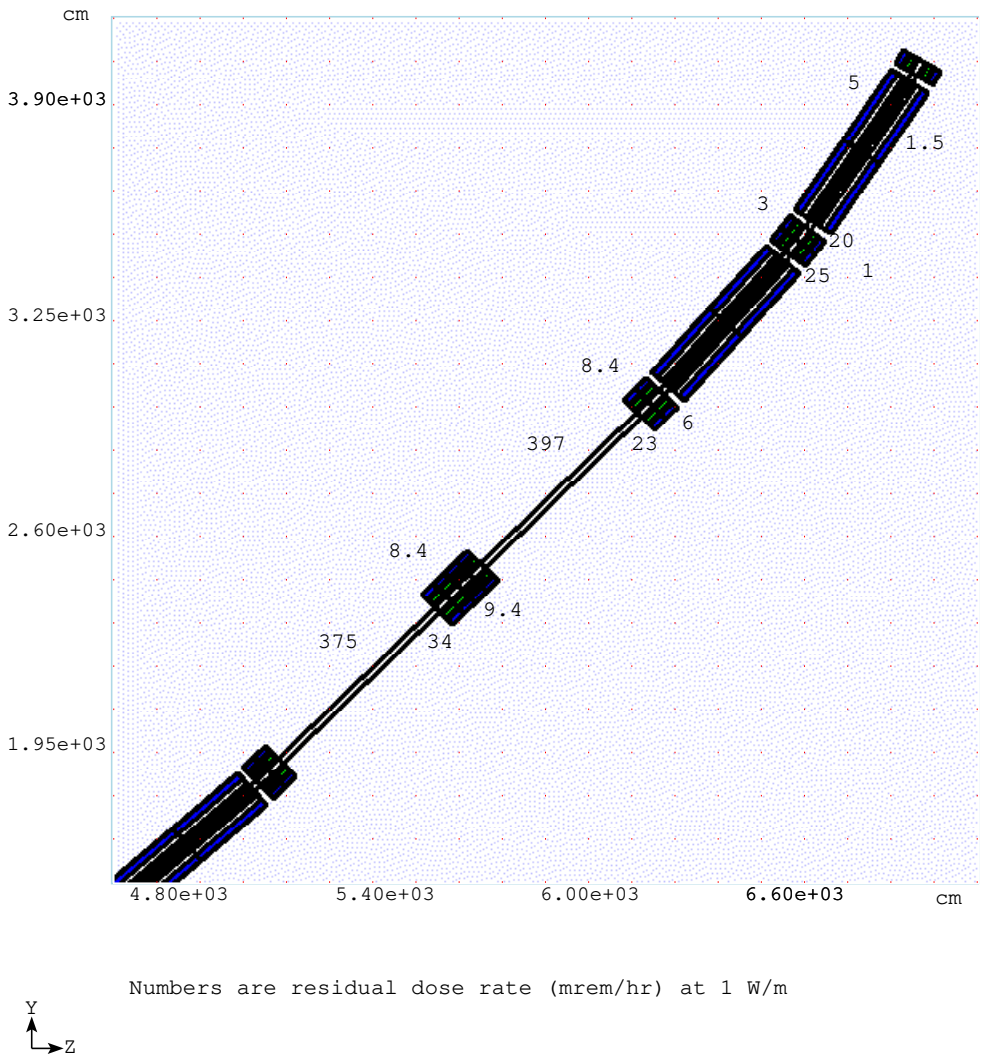

Figure 6: Peak residual dose rates (mrem/hr) on the outer surface of the arc elements at 1 W/m uniform beam loss rate in the 16 GeV Proton Driver.

be adequately protected. Peak accumulated dose in the coils is about 2 Mrad/yr at 1 W/m beam loss rate which is acceptable with use of appropriate materials for insulation. Care should be taken of the cable insulation, possible oil and electronics in the tunnel.

At 16 GeV the determining factor is hands-on maintenance with about 3 W/m as a tolerable maximum beam loss rate in the lattice elements, except for the open long beam pipes where one should reduce the loss rate to 0.25 W/m to reduce the dose to 100 mrem/hr. One needs further reduction to bring the dose down to a good practice value of about 10-20 mrem/hr. Alternatively, one can think of providing simple shielding around the bare beam pipes.

4 Collimation at 16 GeV

The 16-GeV beam power is 1.152 MW. Assuming that 1% of the beam is lost at "slow" growth of the beam size at the top energy, this amounts to 11.52 kW of beam loss. A corresponding 16-GeV beam loss distribution in the ring calculated with the STRUCT code (Fig. 7) shows peak loss up to 3 kW/m on several quadrupoles that is up to 5000 times higher than the allowable limit for ground-water activation.

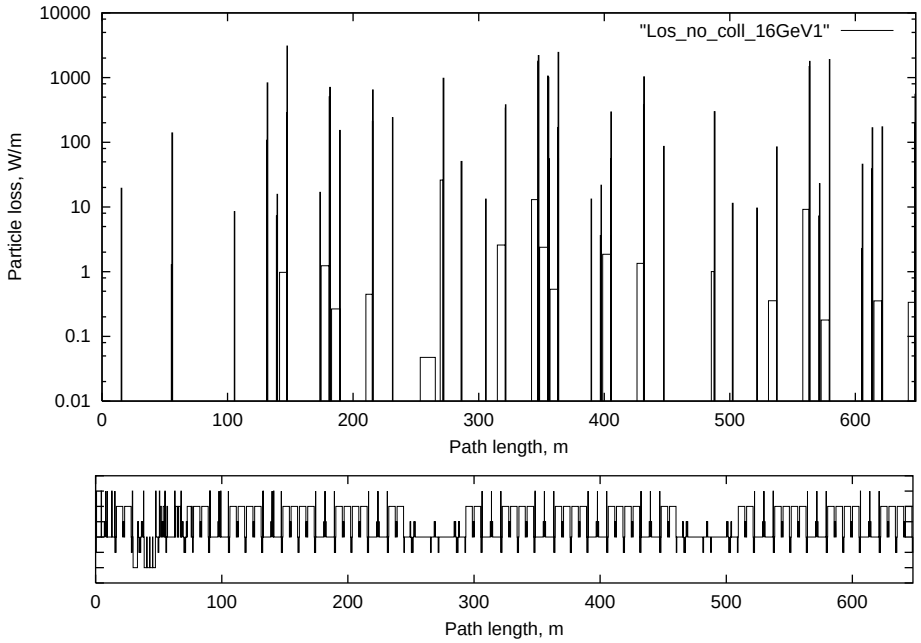

Figure 7: Beam loss distribution without collimators at 1% loss of intensity.

The purpose of the beam halo cleaning system is to localize proton losses in a specially shielded short section, thus to reduce irradiation of the rest of the machine to the acceptable level. A two-stage beam collimation system is designed using the available spaces in the utility section. It consists of horizontal *prim.coll-H* and vertical *prim.coll-V* primary collimators and secondary collimators COLL-1 through COLL-5 as shown in Fig. 2.

For stable operating conditions, a circulating beam size grows very slowly with a small step size per turn. The corresponding proton impact parameter on a primary collimator is of the order of few μm. A thin primary collimator (scatterer), introduced into the lattice as a limited aperture, increases proton amplitude as a result of multiple Coulomb scattering and thus results in drastic increase of impact parameter on the downstream secondary collimators. This results in a significant reduction of the out-scattered proton yield and total beam loss in the accelerator, decreases collimator jaws overheating and mitigates requirements to the collimator alignment [5, 11].

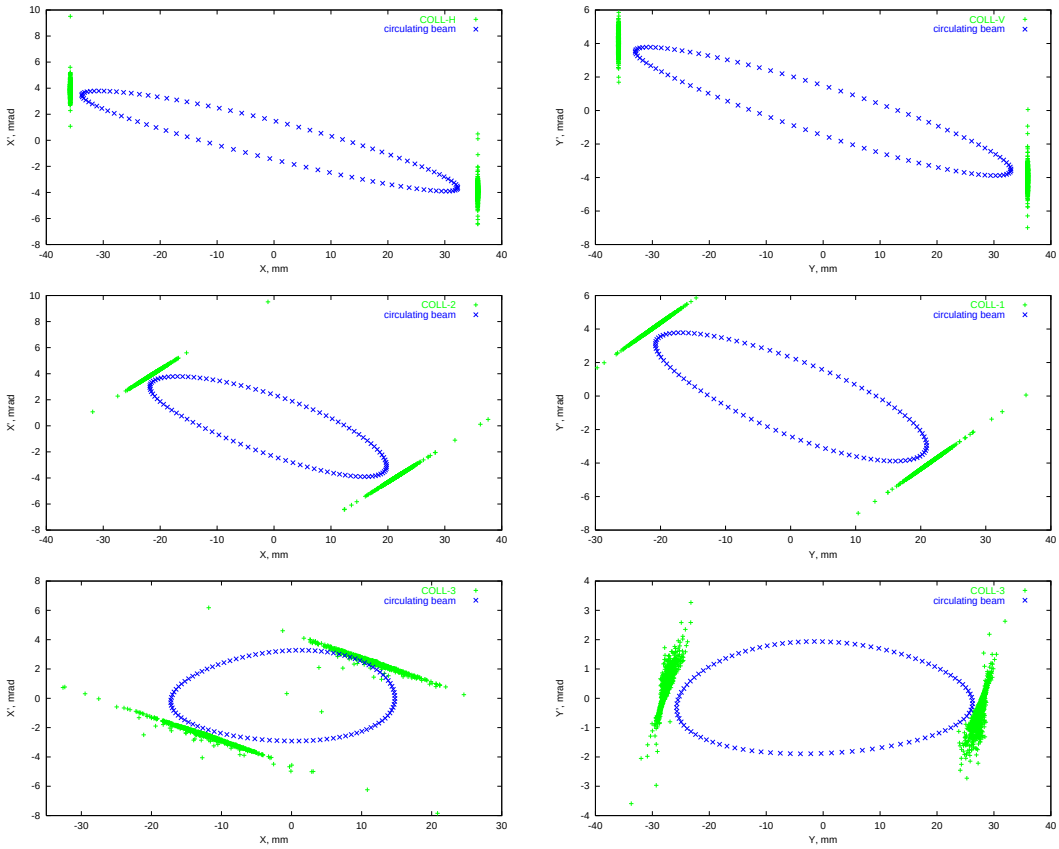

Figure 8: Horizontal (left) and vertical (right) phase space at the primary collimators (first row), secondary collimators COLL-1 and COLL-2 (second row), and at COLL-3(third row).

Table 3: β-functions at the collimators and phase advance between the primary and secondary collimators.

Collimator	β-function (m)		Phase advance (deg)	
	horizontal	vertical	horizontal	vertical
Vertical primary	3.8	22.2	-	0
Secondary COLL-1	13.1	8.8	-	17
Horizontal primary	22.2	5.4	0	-
Secondary COLL-2	8.8	19.1	17	92
Secondary COLL-3	5.2	13.5	134	187
Secondary COLL-4	25.0	9.8	189	224
Secondary COLL-5	13.8	26.4	221	261
Supplementary COLL-6	17.4	28.0	233	267
Supplementary COLL-7	17.4	27.8	245	278

Several primary and secondary collimators have been introduced into the Proton Driver utility section. Secondary collimators need to be placed at phase advances which are optimal to intercept most of particles out-scattered from the primary collimators during the first turn after the halo interaction with the primary collimator. Transverse phase space at the collimators is shown in Fig. 8. The optimal phase advance is around $k \cdot \pi \pm 30^o$. Phase advances between the Proton Driver primary and secondary collimators are presented in Table 3. The horizontal secondary collimators 2, 3 and 4 and vertical collimators 1 and 3 have good phase advances with respect to the primary collimator. The horizontal and vertical primary collimators are placed at the edge of the beam after painting. Beam loss distributions at 16 GeV with secondary collimators located at all the possible free drift spaces of the collimation section at various distances from the beam edge are shown in Fig. 9. It is assumed in calculations that 0.66% of the 16-GeV beam is lost on the horizontal primary collimator (a half for off-momentum protons with $\Delta p/p = \pm$ 0.002 and a half for on-momentum protons) and 0.33% is lost on the vertical primary collimator.

Secondary collimators still generate out-scattered particles lost later in the lattice. One can eliminate or at least reduce this component with a *3-stage collimation system* positioning several *main* secondary collimators close to the beam to deal with protons scattered in the primary collimator and several *supplementary* collimators farther from the beam to catch particles out-scattered from the main secondary collimators. Beam loss distributions for several considered combinations are shown in Fig. 9. A few inefficient secondary collimators have been removed from the system in the course of this optimization. The minimum number of secondary collimators is five, but additional collimators COLL-6 and COLL-7 further reduce (slightly) beam loss in the ring. One can see significant reduction of beam loss rates with the proposed *3-stage collimation system*. Table 4 summarizes results of this optimization for a 1-mm thick tungsten primary collimator and 0.3-m long steel secondary ones.

The thickness and material of primary collimators affect the out-scattered proton angular distribution and nuclear interaction rate in it. Such a thin scatterer should give a considerable angular kick to the halo particles, but their amplitude should remain smaller than the machine aperture on their way to the secondary collimators. Calculated beam losses are presented in Table 5 for 0.5, 1, 2 and 4 mm thick tungsten collimators with 0.3-m secondary collimators COLL-1,2,3 at 0.5 mm, COLL-4,5 at 2.5 mm, and with additional collimators COLL-6,7 at 6.5 mm from the beam edge. Total loss is 11.52 kW. A 1 mm collimator provides minimal peak loss rate in the ring. The β-function varies along the length of a secondary collimator, therefore the collimator apertures are assumed to be tapered follow the beam envelope after the painting. Longer secondary collimators reduce the punchthrough probability and we found that at 16 GeV the minimal length is 0.3 m of steel, with the optimum of 0.3-0.5 m (see Table 6). The results shown are for a 1 mm thick tungsten primary collimator and for the secondary and supplementary collimator positions as above.

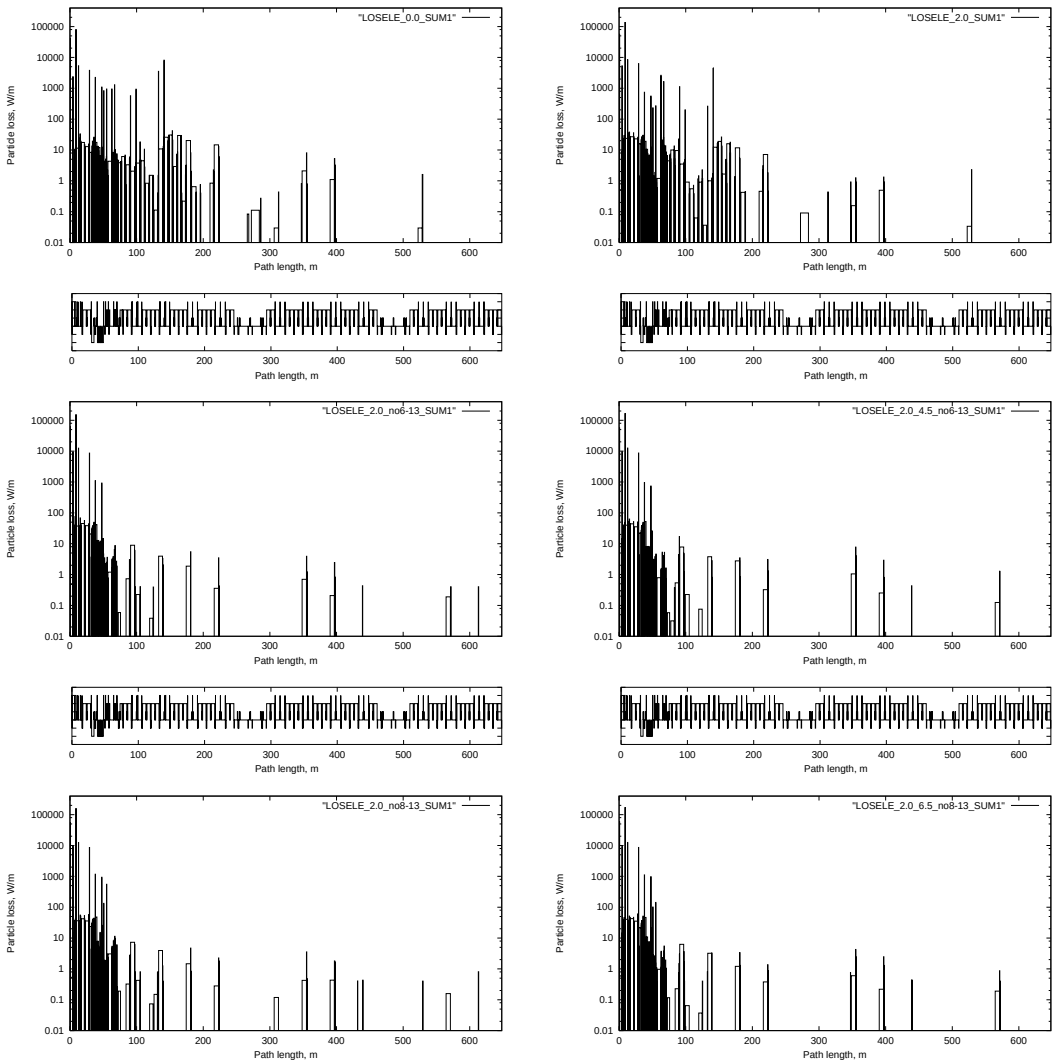

Figure 9: 16-GeV beam loss distributions with a 1 mm thick tungsten primary collimators at the edge of the beam after painting. *Top, left*: thirteen secondary collimators are at 0.5 mm from the beam edge. *Top, right*: COLL-1,2,3 are at 0.5 mm, others are at 2.5 mm from the beam edge. *Middle, left*: COLL-1,2,3 are at 0.5 mm, COLL-4,5 are at 2.5 mm. *Middle, right*: COLL-1,2,3 are at 0.5 mm, COLL-4,5 are at 4.5 mm. *Bottom, left*: COLL-1,2,3 are at 0.5 mm, COLL-4,5 are at 4.5 mm, with additional collimators COLL-6,7 at 4.5 mm. *Bottom, right*: COLL-1,2,3 are at 0.5 mm, COLL-4,5 are at 4.5 mm, COLL-6,7 at 6.5 mm.

With the proposed system, $\sim$99% of the beam halo energy is intercepted in the 60-m long utility section. About 1% is lost in the rest of the machine along 588 m length with the mean rate of 0.2 W/m. At several locations the beam loss is noticeably higher ($\sim$6.3 W/m), exceeding the tolerable rates of Table 2. One should notice

Table 4: Beam loss in the 16 GeV Proton Driver. Total loss is ∼11.52 kW.

Collimator		Beam loss		
Name	Position	60-m Utility section	Rest of the ring	Peak loss rate in the ring
	mm	kW	kW	W/m
No collimators	-	0.0965	11.42	3070
Primary COLL-1 – 13	0.0 0.5	5.69	5.82	42
Primary COLL-1 – 3 COLL-4 – 13	0.0 0.5 2.5	7.62	3.90	18
Primary COLL-1 – 3 COLL-4 – 5	0.0 0.5 2.5	11.38	0.149	8.9
Primary COLL-1 – 3 COLL-4 – 5	0.0 0.5 4.5	11.39	0.142	7.8
Primary COLL-1 – 3 COLL-4 – 5 COLL-6 – 7	0.0 0.5 2.5 4.5	11.35	0.169	11.4
Primary COLL-1 – 3 COLL-4 – 5 COLL-6 – 7	0.0 0.5 2.5 6.5	11.41	0.1116	6.3
Primary COLL-1 – 3 COLL-4 – 5 COLL-6 – 7 with bump at primary	0.0 0.5 2.5 6.5 6.5 6.5	11.50	0.0208	5.0

here that these results are for an ideal machine. Orbit and tune variation can change the numbers somewhat. A corresponding sensitivity analysis will be performed at the next stage. The above 'hot' locations should be taken care of via local shielding. Beam loss rates in the collimation system section itself are very high implying a special shielding design (see Section 7). Collimators, magnets and other equipment of the utility section require special cooling as well as fast disconnects and remote control.

Table 5: Beam loss as a function of thickness t of a primary tungsten collimator.

t	60-m Utility section	Rest of the ring	Peak loss rate in the ring
mm	kW	kW	W/m
0.5	11.400	0.1194	8.4
1.0	11.408	0.1116	6.3
2.0	11.404	0.1160	7.2
4.0	11.412	0.1085	8.4

Table 6: Beam loss as a function of length L of secondary steel collimators.

L	60-m Utility section	Rest of the ring	Peak loss rate in the ring
m	kW	kW	W/m
0.2	11.224	0.2960	25.2
0.3	11.408	0.1116	6.3
0.5	11.452	0.0676	6.0
0.8	11.471	0.0486	5.7

5 Collimation at Injection and Acceleration

It is assumed that 10% of intensity is intercepted at injection, and 1% at the top energy. A practicality in a rapid cycling proton synchrotron dictates a stationary collimator approach with collimator jaws in a fixed position with respect to the beam orbit during the entire cycle. In the optimal configuration described in the previous section, the primary collimators are positioned at the edge of the beam after beam painting in the horizontal and vertical planes with the secondary and supplementary collimators farther from the beam.

In an ideal case, the edge of the circulating beam should be kept at such conditions during the total cycle. This requires rather complicated horizontal and vertical bumps, created by ten fast magnets for each direction. To simplify the system, we propose to keep the beam at the edge of the primary collimators and close to the first secondary collimators using only three fast magnets for each direction. Most of the particles scattered out of the primary collimators are intercepted now by these secondary collimators, with other collimators intercepting the larger amplitude and off-momentum protons. Such a scheme allows to localize a majority of the beam loss in a short 15-m long region with the maximum rate of 140 W/m in the quadrupole immediately downstream of COLL-1. Corresponding beam loss distributions at 400-MeV injection and at the top energy are shown in Fig. 10 and in Table 4. The peak loss rates in the ring downstream of the utility section with such a bump are 5 W/m at 16 GeV and about 0.1 W/m at injection.

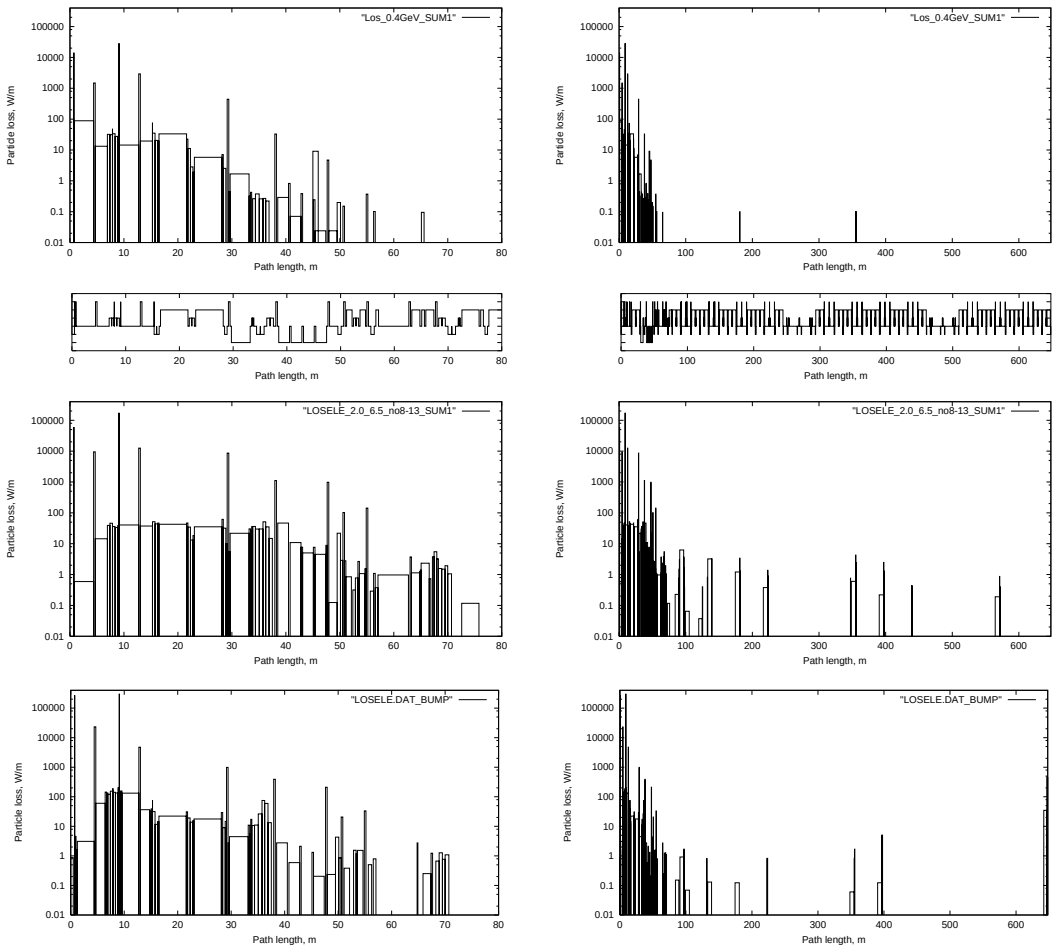

Figure 10: Beam loss in the utility section (left) and in the entire ring (right) at injection (top), at the top energy without bump (middle) and with the proposed bumps (bottom).

6 Beam Collimation at RF Capture

Beam losses at the RF capture were simulated using difference equations for proton motion with respect to the synchronous particle [12]:

$$\varphi_i = \varphi_{i-1} - 2\pi \cdot f_{RF} \cdot f_{rev}^{-1} \left[\alpha - \frac{1}{\gamma^2} \right] \frac{\Delta E}{\beta^2 \cdot E_s}, \tag{3}$$

$$E_{exit} = E_{entrance} + \frac{U}{1000} \left[\sin(\varphi_I) - \sin(\varphi_s) \right], \tag{4}$$

where

φ_I is a proton RF phase at the RF station (radian);

φ_{I-1} is a proton RF phase at the previous turn (radian);

φ_s = 0.087266 is the synchronous phase at the beginning of acceleration;

E_s = 1338.3 MeV is the synchronous energy;

f_{RF} = 1.2×10^6 Hz is the RF frequency at the beginning of acceleration;

f_{rev} = 0.3×10^6 Hz is the revolution frequency at injection;

α = -0.000744 is the momentum compaction factor; one neglects the dependence of α on proton momentum;

$\gamma = E_s/(m_o \times c^2)$ = 1.4263 is the γ factor;

$e \times U$ = 1.2 MeV, U is the RF voltage.

A longitudinal phase space is shown in Fig. 11. The maximum energy deviation from the synchronous energy in the bucket and the frequency of synchrotron oscillations at injection are ΔE = 15 MeV and f_{synchr} = 7 kHz, respectively. The duration of synchrotron oscillation is 43 turns. In these simulations the initial protons were placed in the vicinity of an unstable point. Fig. 12 shows evolution of the longitudinal phase space. Corresponding transverse distributions at the primary collimator and momentum spectrum of the lost protons are shown in Fig. 13. Most halo protons on the primary collimator have $\Delta p/p \leq 1\%$. Beam losses at injection in the utility section and in the entire ring are presented in Fig. 14 for the beam size growing slowly on the primary collimator (20 μm) and for beam loss at the RF capture with a step size of 3 mm. Maximum dispersion in the ring is equal to 5.3 m, compared to the dispersion at the primary collimator of 4.6 m. This results in slightly increased beam loss in the ring for the off-momentum protons compared to the losses at the amplitude growth.

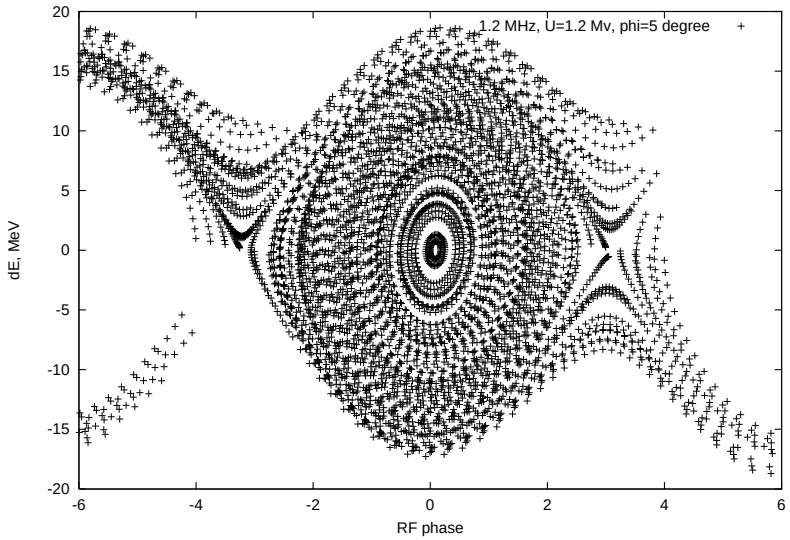

Figure 11: Longitudinal phase space at RF capture.

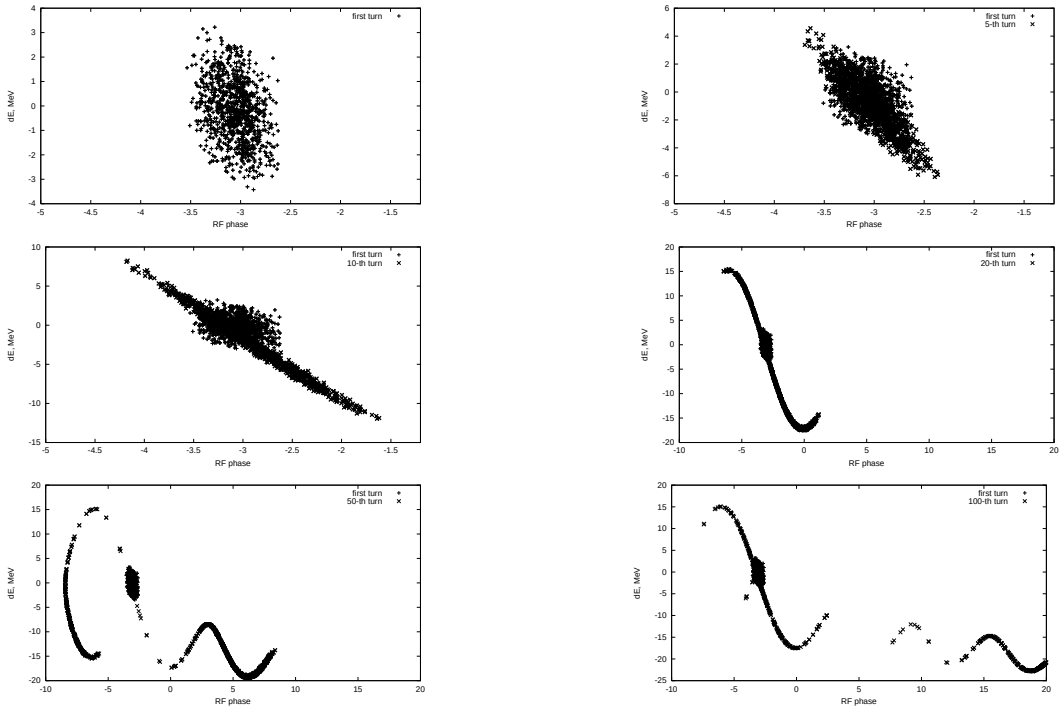

Figure 12: Longitudinal phase space at RF capture at the 1-st (top, left), 5-th (top, right), 10-th (middle, left), 20-th (middle, right), 50-th (bottom, left) and 100-th (bottom, right) turns. Initial protons are in the vicinity of the unstable point.

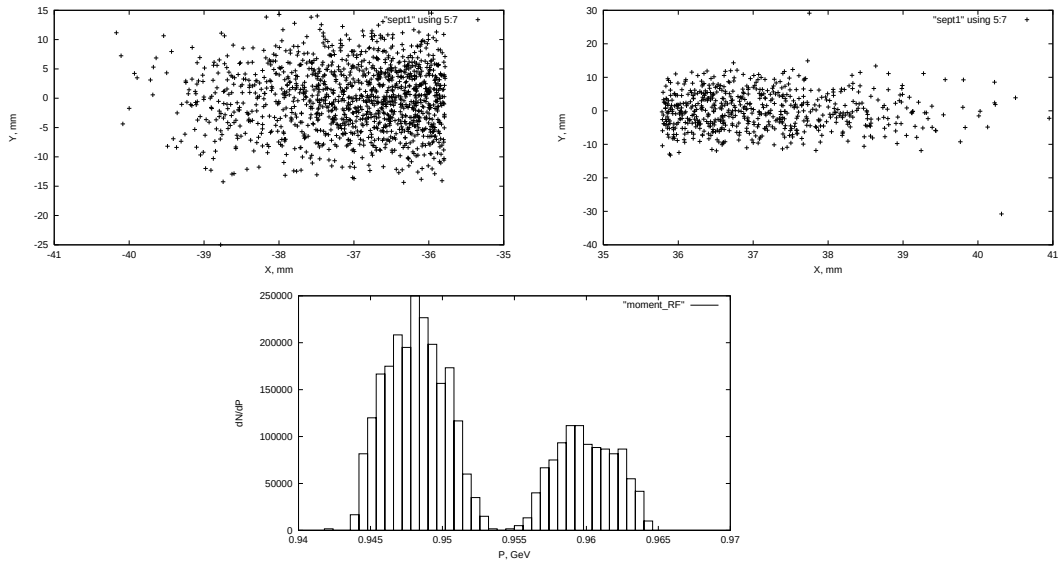

Figure 13: Transverse distributions of halo protons on the primary collimators (top) and momentum spectrum of lost protons (bottom) during the RF capture.

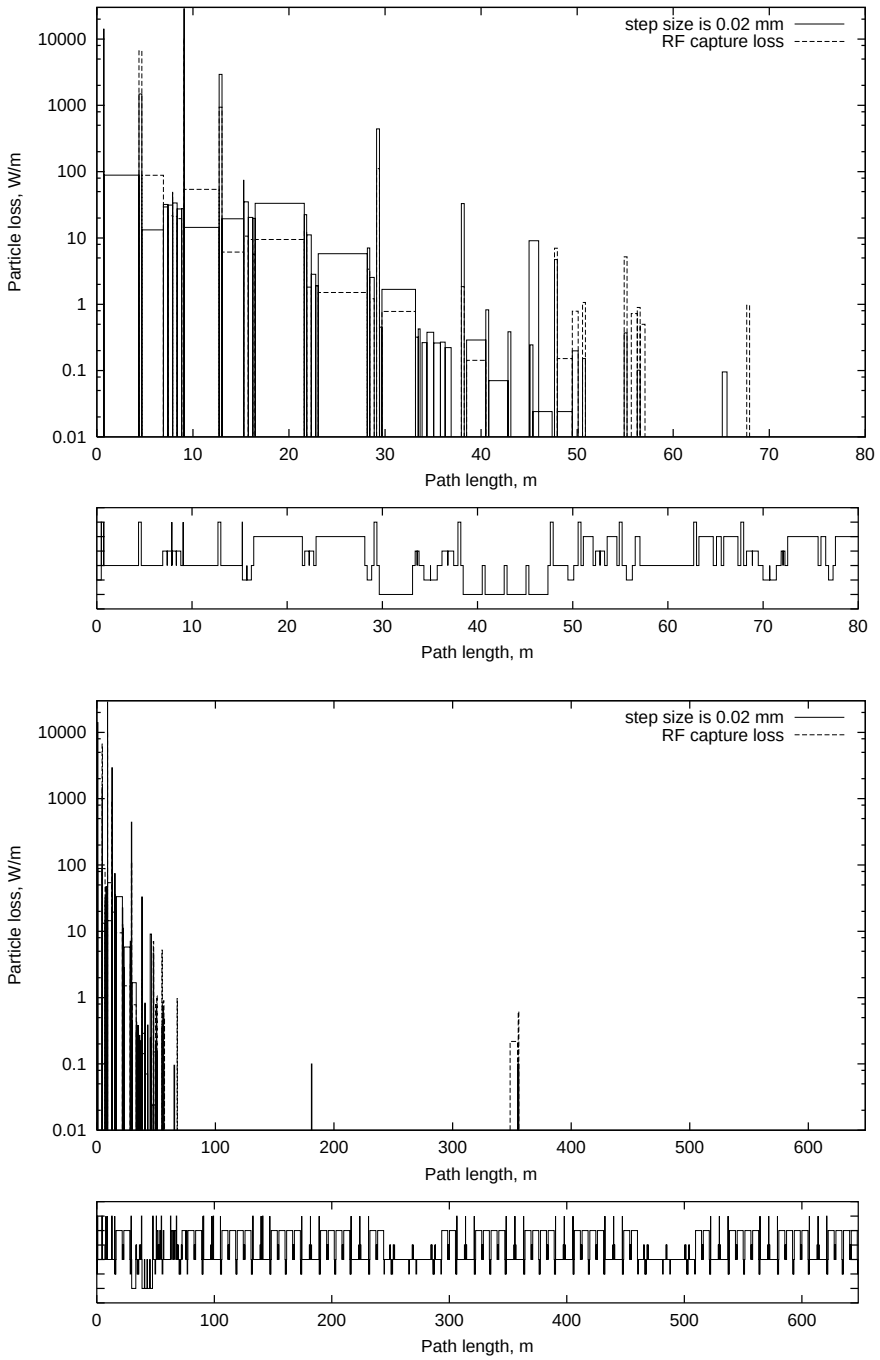

Figure 14: Beam losses at injection in the utility section (top) and in the entire ring (bottom) for the the beam size on the primary collimator growing slowly (solid line) and at the RF capture with a step size of 3 mm (dashed line).

7 Crystal Collimation

In this section we explore a possibility to use a crystal instead of an amorphous primary collimator, studied earlier for the Tevatron beam scraping system [13]. To evaluate an efficiency of such a collimation system, realistic simulations have been performed with STRUCT linked to the CATCH code [14]. Crystal channeling is simulated in CATCH as described in Ref. [15]. Interactions with a crystal amorphous layer and all other near-beam interactions and tracking are performed with STRUCT.

An optimal Si(110) crystal radius is estimated as $R(mm) \approx 30 \times p\beta$, where p is a proton momentum (GeV/c) and β is its velocity relative to the speed of light. Corresponding crystal length needed to deflect a proton by an angle θ is $L = R\theta$. A 3-mm silicon crystal deflects 16-GeV protons by 5.9 mrad. A crystal critical angle, estimated as $\alpha(mrad) \approx 0.15/\sqrt{p\beta}$, is 0.18 mrad at injection and 0.036 mrad at 16 GeV. To channel, these angles should be much larger than a beam divergence. Another parameter, especially important at low energies, is a crystal dechanneling length $L_{dechan}(mm) \approx p\beta$, that is 0.7 mm at 400 MeV and 17 mm at 16 GeV. In a rapid cycling machine the same crystal should be used both at injection and at the top energy, and it is clear that the requirement $L < L_{dechan}$ is violated at injection.

In this study the attempt was made to replace the primary collimator with a silicon crystal with a 1 μm thick amorphous layer on the beam-side of the crystal. The beam half-size at the crystal is 35.8 mm horizontally. The beam amplitude can grow rapidly due to the space charge effects. Let's assume that a proton impact parameter at the crystal is about 30 μm. Then a corresponding beam divergence at the crystal entrance (Fig. 15) is ± 50 μrad independently of the beam energy.

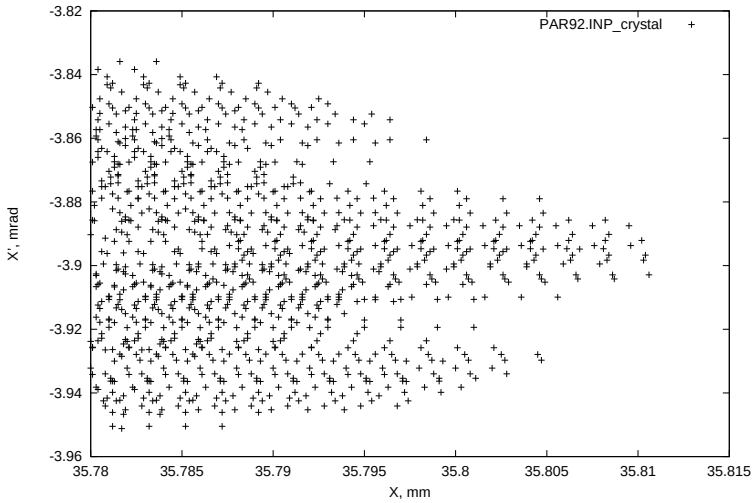

Figure 15: Horizontal phase space at the crystal.

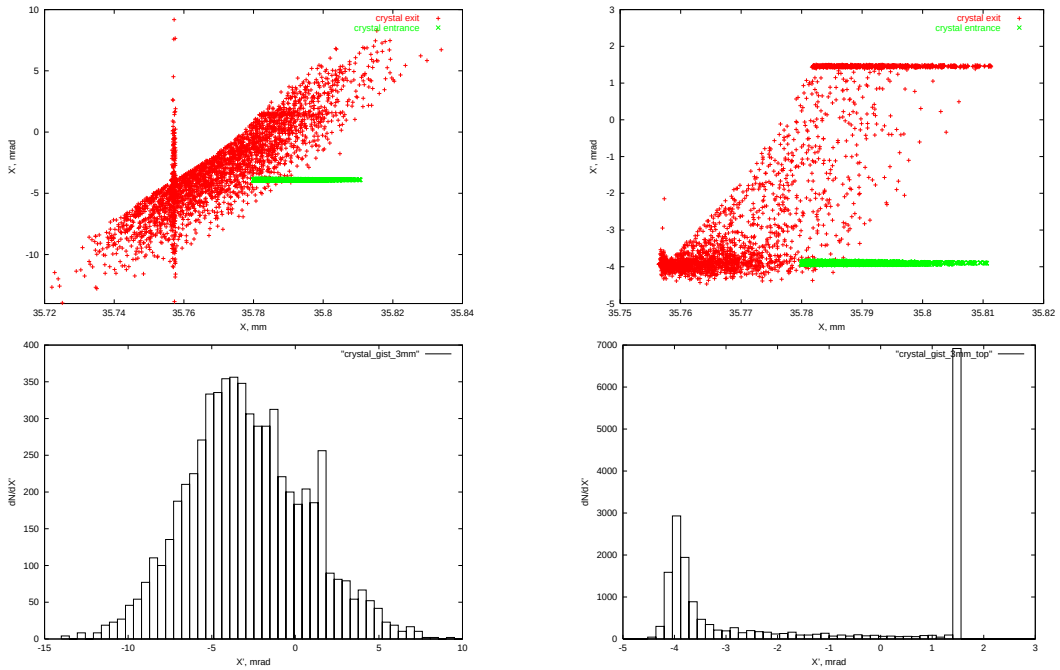

Figure 16: Horizontal phase space at a 3-mm crystal entrance and exit (top), and angular distribution at the crystal exit (bottom) at injection (left) and at 16 GeV (right).

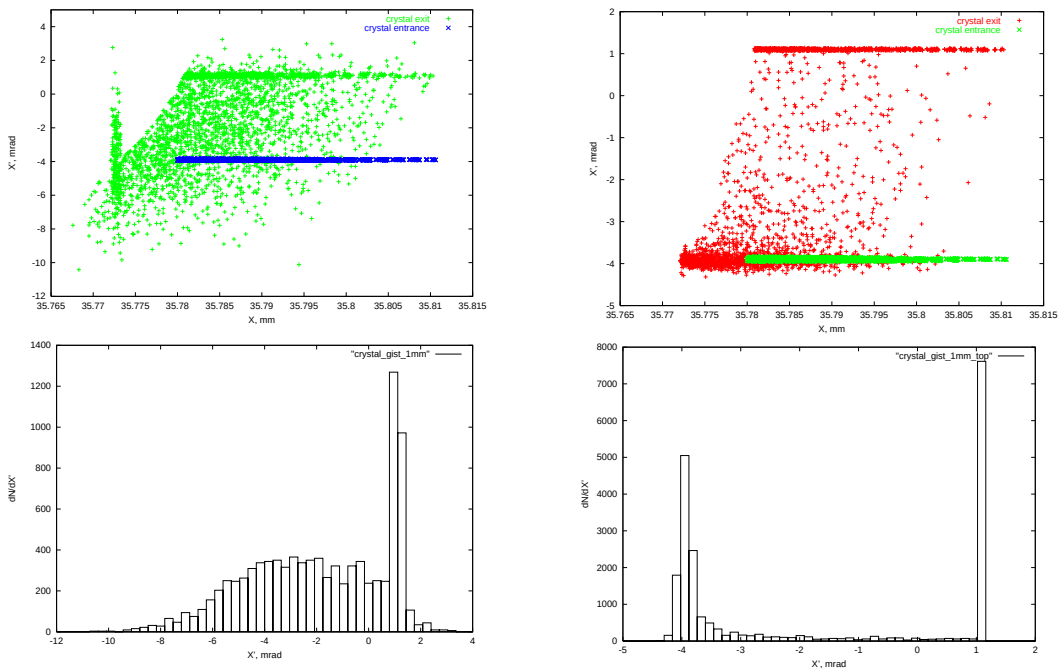

Figure 17: Horizontal phase space at a 1-mm crystal entrance and exit (top) and angular distribution at the crystal exit (bottom) at injection (left) and at 16 GeV (right).

Beam distributions immediately upstream and downstream of a 3 mm silicon crystal are shown in Fig. 16. With this crystal $L < L_{dechan}$ at the top energy, but the beam divergence exceeds the critical angle. Therefore, the channeling efficiency on the first pass is 37% only. At injection—although a critical angle (180 μrad) is larger than the beam divergence—the efficiency is even lower than about 7%, because of a very short dechanneling length.

Nowadays technologies allow to bend a 1-mm crystal by 1-2 mrad, with a hope to increase this angle to 5 mrad in the near future. This would reduce dechanneling and nuclear interactions in the crystal resulting in a higher channeling/collimation efficiency. We have just tried such a crystal in our simulations. Fig. 17 gives beam distributions with a 1-mm silicon crystal bent by 5 mrad. Calculated channeling efficiency on the first pass is now 35% at 16 GeV and 27% at injection. A factor of four increase at injection is very encouraging. Unfortunately, at the top energy, many protons are not channeled by a short crystal (see Fig. 17).

Beam loss rates with such a crystal are compared with those using an amorphous primary collimator in Fig. 18 for the utility section. The multiple Coulomb scattering angle at injection in the 1 mm thick tungsten is quite large (θ_{mcs}=8 mrad) compared to the dechanneling angle in the silicon crystal (Fig. 17). Therefore the losses with the crystal are lower compared to the the baseline case with an amorphous tungsten scatterer by an order of magnitude. At the top energy, the situation is inverse (θ_{mcs}=0.6 mrad), resulting in about a factor of four higher losses in the utility section at crystal collimation despite of a rather high channeling efficiency. If the beam loss at the top energy is much less than that at injection (compared to the assumed 1:10 ratio), the crystal collimation could be a good possibility for the collimation system improvement.

Radiation damage to the crystal will limit its use in high-intensity beams. At high dose, the irradiated layers become amorphous. The experiment at CERN SPS at 450 GeV has shown the crystal efficiency reduction by 6% at 10^{18} particles per mm^2 [15, 16]. A limiting flux at 800 GeV beam at Fermilab was found to be 10^{19} particles per mm^2 [17] At lower energy the crystal is less sensitive to the crystal lattice damage with an acceptable angular distortion changing as $1/\sqrt{p\beta}$ [16]. Assuming a step size due to a space charge effect of 0.020 mm/turn, one gets a beam size on the crystal of 20 mm$\times$0.020 mm. The proton flux through the crystal is then 4.5×10^{17} p/mm^2/hr at 3.3×10^{12} protons lost per the accelerator cycle. Assuming radiation hardness of the crystal at 16 GeV of 7×10^{19}p/mm^2, the crystal lifetime is estimated as 160 hours. In the rapid cycling machine the RF capture loss can be the main component to be collimated. Step size in this process is equal to 3 mm/turn. With that, the proton flux through the crystal is 3×10^{15} p/mm^2/hr. It gives 2.7 years for the crystal lifetime.

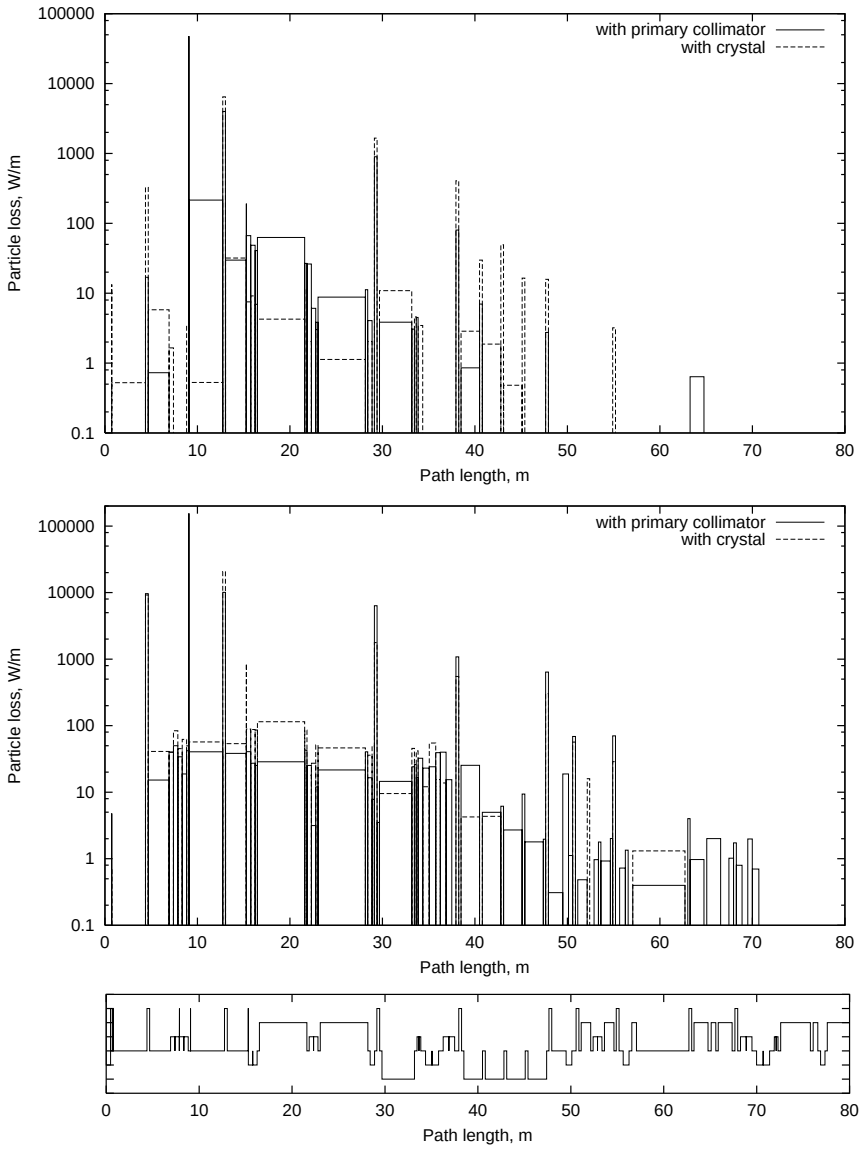

Figure 18: Beam loss in the utility section at injection (top) and at the top energy (bottom) for the systems with a 1-mm tungsten primary collimator (solid line) and with a 1 mm silicon crystal (dashed line).

8 Radiation Shielding

8.1 Design Criteria

The shielding analysis for the arcs and utility section is performed both for normal operation and for accidental beam loss. A simplest operational scenario is a 1 W/m beam loss rate distributed uniformly along the arc lattice, while the realistic one is

that based on the beam loss distributions calculated in the previous sections, with the average rates in the arcs of about 0.2 W/m at the top energy and less than 0.05 W/m at injection. In both cases, beam loss and local shielding (see below) in the collimation region are determined from the realistic distributions in the utility section calculated in this study. With the long bare drifts in the arcs and utility section components locally shielded to meet hands-on maintenance limits, the ground-water protection requirements are fulfilled (see 3.4). Certainly, a 4 MW second stage of this project would require further consideration of radiation shielding issues. Prevention of ground-water flow in a vicinity of the tunnel wall is an additional possibility here. The shielding against prompt radiation should be designed such that the dose rate on accessible outer surfaces of the shield is less than 0.25 mrem/hr in non-controlled areas.

For the worst case catastrophic *incredible* accident we assume a loss of the full 1.2 MW of beam at a single point for an hour, with the shielding reducing the dose on accessible outside surfaces of the shield to less than 5 mrem in non-controlled areas. The new DOE regulations now allow for credit to be taken for active shutdown measures, allowing one to address *credible* beam spill accidents with respect to the shield design [18]. The work is underway at Fermilab towards the "worst credible accident" approach, which would allow to limit the amount of beam lost in such an accident to about 0.1% of that in the *incredible* case.

8.2 Benchmarking

Reliable calculation of dose attenuation in the shielding to the above levels is a non-trivial problem. Several techniques—such as biasing, mathematical expectation, exponential transformation and a combination of Monte Carlo with deterministic methods—are used to reach probability levels of $\sim 10^{-10}$. The uncertainties of the radiation field predictions in such a dynamic range are not easy to quantify. The most direct way is benchmarking against the evaluated experimental data or other reliable simulation codes.

There has been a substantial progress with Monte-Carlo code developments and validation over last several years. The current versions of the MARS [8], FLUKA [19, 20] and MCNPX [21] codes are obvious leaders. These days, if the right person uses the right code, energy deposition, particle fluxes and related values can be predicted with a 10% accuracy in a majority of cases. Residual dose rate calculation uncertainty is within a factor of two. This is fully true for the related problems and energy domain of the Proton Driver.

Recently, two code verifications have been performed with the independent calculation methodologies. The first was for a simplified model of the SNS Linac tunnel [22]. A section of the tunnel was modeled as a cylindrical shell of concrete 2.3 m in radius, 0.46 m thick and 30 m long. The tunnel was filled with air and surrounded by 9 m of earth berm for shielding. A 0.15 m diameter by 1 m cylinder

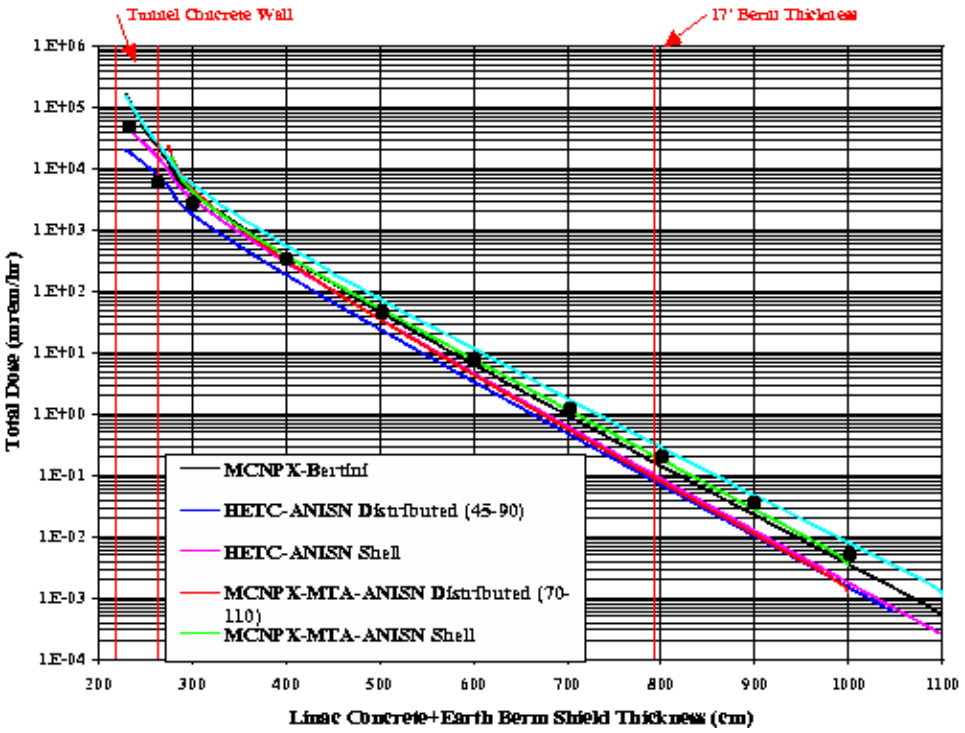

Figure 19: Dose attenuation in the ORNL SNS Linac earth berm [22] as calculated by ORNL group (lines) and with MARS14 (symbols).

of copper was modeled in the center of the geometry to simulate the interaction of the 1 GeV proton beam with accelerator components. The ORNL, BNL and FNAL teams provided their results for this benchmarking. Fig. 19 shows dose attenuation in the earth berm predicted in six different approaches. The FNAL results obtained with the MARS code [7, 8] closely match the ORNL ones obtained with the most recent version of the LANL MCNPX-CEM code [21] and are within a factor of two of the "recommended" MCNPX-BERTINI results.

Another recent benchmarking [23] was performed for a 2-m long cylinder—representative of the forward shielding of the CMS detector at LHC—for a 10 GeV/c pencil proton beam hitting it. The absorber consisted radially of iron ($0< r <40$ cm), concrete ($40< r <100$ cm), borated polyethylene ($100< r <110$ cm) and air at $110< r <120$ cm. Fig. 20 shows almost perfect agreement of MARS14 and FLUKA [19] for energy-integrated neutron fluxes. Both codes reproduce similarly the physics of interactions in different materials in the energy range spanning from tens of GeV down to a fraction of an electronvolt.

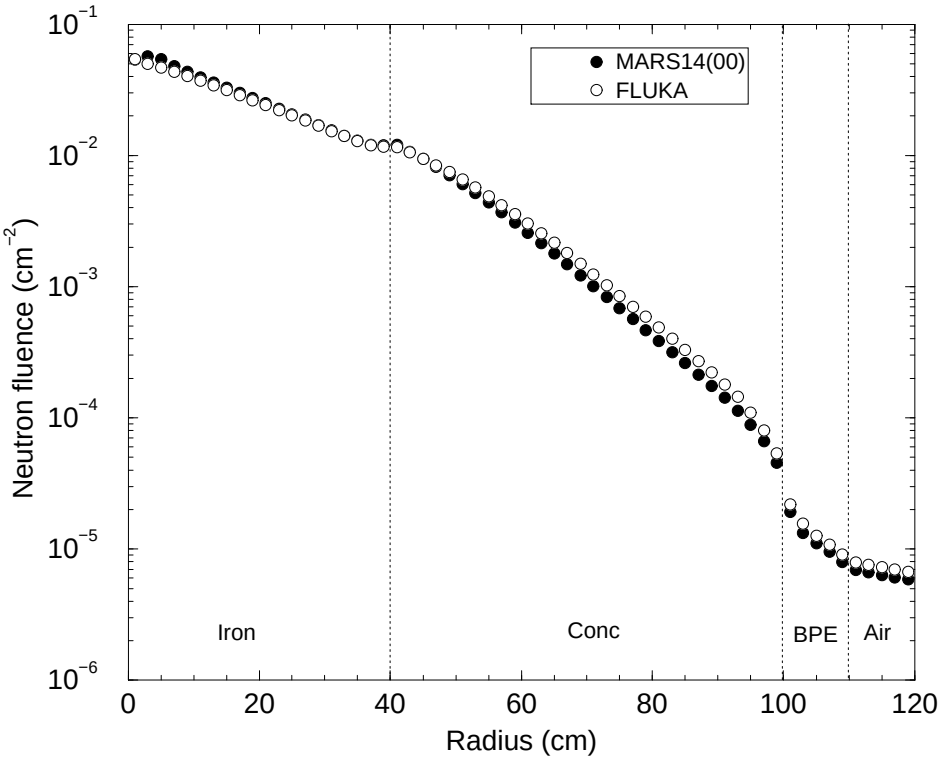

Figure 20: Total neutron fluence at 50$< z <$100 cm in a 2-m composite cylinder irradiated by a 10 GeV/c pencil proton beam as calculated by MARS14 and FLUKA.

8.3 Arcs

Full 3-D calculations of beam loss and showers induced in a 84-m arc cell were performed with the MARS14 code. Beam loss and geometry models are described in Sec. 3.3. In addition to detailed lattice description with dipoles, quadrupoles and drifts (see Figs. 3 and 4), a simplified tunnel surrounded with the dirt shielding (Fig. 21) was implemented into the code. Both longitudinally uniform beam loss and a point-like accidental beam loss inside the arc magnet were simulated in this model. Fig. 22 shows the dose calculated as a function of the thickness of the dirt shielding (ρ=2.24 g/cm^3) for a point-like loss of a 16-GeV proton. The dose which corresponds to the 5 mrem limit for the worst case catastrophic *incredible* point-like loss of 3.0×10^{13} protons for an hour is D_0=3.09×10^{-23} Sv per proton (1 Sv = 100 Rem). At the same conditions, at 0.4 GeV with 3.3×10^{13} protons per pulse, D_0=2.81×10^{-23} Sv per proton. Corresponding thicknesses of the dirt shielding around the tunnel are 26 and 17 feet, at 16 and 0.4 GeV respectively. With the beam loss in a *credible* accident at 0.1% of the above, the shield thickness at 16 GeV is reduced to 16 feet.

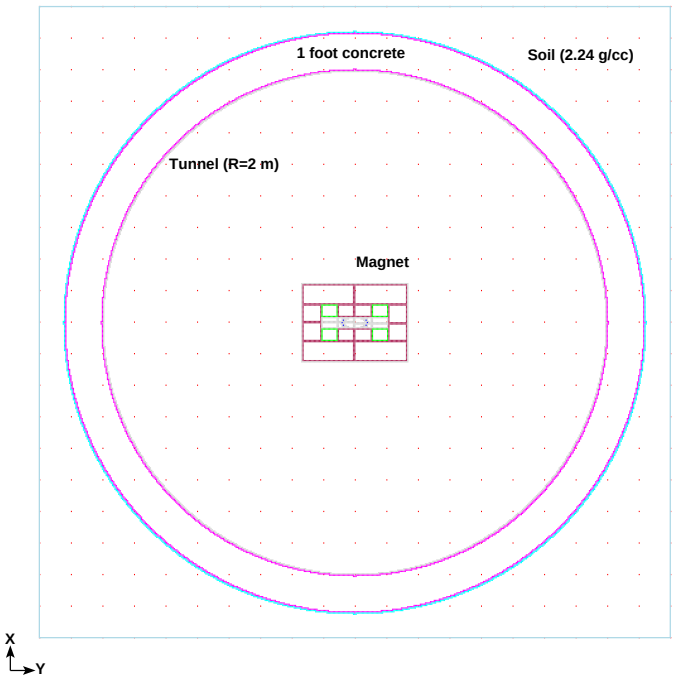

Figure 21: Simplified MARS model of the arc tunnel.

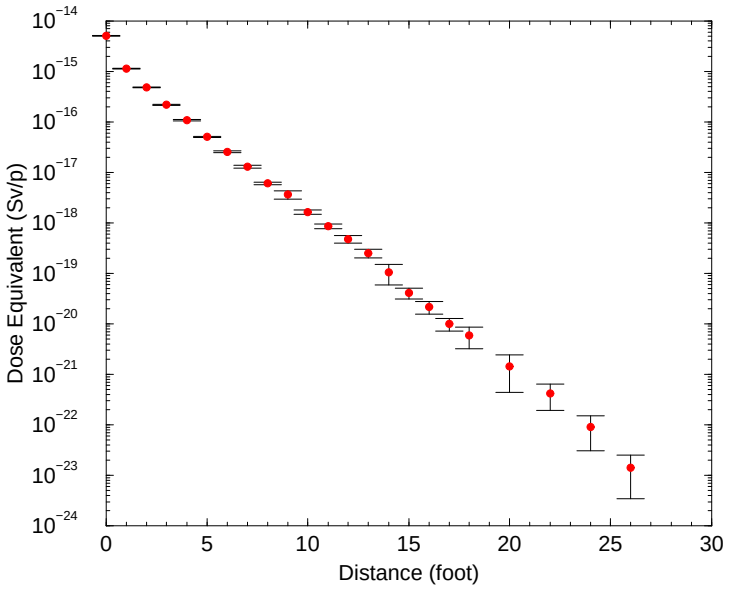

Figure 22: Prompt dose equivalent *vs* dirt thickness around the tunnel at a point-like loss of a 16-GeV proton.

At normal operation, the shielding required is much thinner of that in the worst case catastrophic *incredible* accident. With the uniformly distributed beam loss rate of 1 W/m in the magnets—which is equivalent to about 3.9×10^8 p/m/s lost at 16 GeV—the dirt shielding thickness needed to reduce the dose to 0.25 mrem/hr is $\sim$12 feet. This thickness is reduced further if one takes into account the average 16 GeV beam loss rates of $\sim$0.2 W/m calculated in Sec. 4, or even lower rates at injection of Sec. 5.

In routine shielding analyses at Fermilab, a simple formula is used [24]. It corresponds to a well-known empirical rule: each meter of dirt decreases the dose by about an one order of magnitude, therefore the thickness y (ft) can be estimated as

$$y = y_1 - s \cdot \log_{10} \frac{D/D_1}{p \cdot N/N_1}, \tag{5}$$

where y_1 (ft) is the dirt thickness to provide dose of D_1=1 mrem/hr at the surface for N_1=10^{13} protons lost locally in an hour, s (ft) is the thickness of dirt required to reduce dose by a factor of ten, D (mrem/hr) is the dose on the surface, N is the number of the protons lost in the cycle and p is the number of cycles per hour. The loss is assumed to be point-like inside the magnet. Under the accidental conditions described above—continuous point-like beam loss for one hour and 5 mrem/hr limit—this formula gives 27 feet of dirt shielding around the tunnel, very close to 26 feet calculated with MARS.

8.4 Utility Section

The utility section with the collimation system intercepting about 99% of beam loss is the hottest region in the machine. Local shielding should be implemented around the collimators and hot magnets downstream to provide residual dose rates on the outside of the shielding less than 100 mrem/hr (roughly equivalent to hadron flux above 20 MeV of 10^6 cm^{-2}s^{-1}). Averaged over the components, the dose rate should be less than 10-20 mrem/hr (a good practice value). Radiation load on ground water around the utility section tunnel should not exceed the allowable limits of Sect. 3. Shielding design will also include material cost/volume minimization as well as civil construction, cooling and remote control.

Beam loss distribution of Fig. 10 is used as a source term in the MARS14 simulations in this region. The collimator parameters are as described in Secs. 4 and 5. In this study only the hottest region is considered which includes all the components at the first 16 meters of the utility section with two primary and two secondary collimators COLL-1 and COLL-2. Out of 1% of the beam intercepted by the collimators at the top energy, two thirds are lost in this region. The secondary 0.3-m long collimators are the hottest spots with beam loss rates up to 13 kW/m.

Calculations show that the optimal configuration would include local shielding around collimators along with extended shielding over the entire region (Fig. 23).

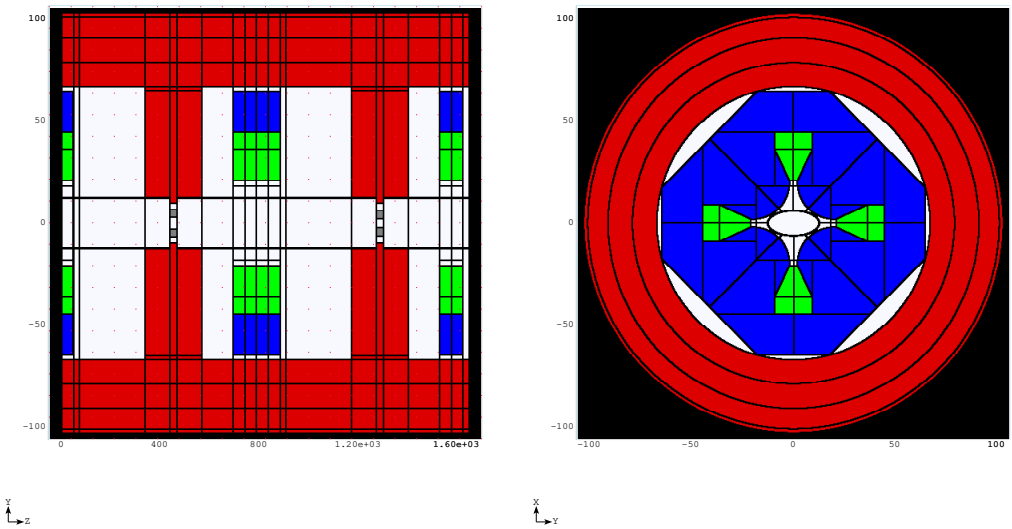

Figure 23: Longitudinal view of the collimation region (left) and cross-sectional view of the quadrupole (right) with the proposed shielding as implemented into the MARS14 calculation model.

Local steel shielding is 2.3 m long and 0.5 m thick transversely around both secondary collimators. Extended shielding around this hot 16-m long section can be made of steel occupying the radial region of $70<r<110$ cm. Residual dose rates on the outer surface of such a shielding (see Fig. 24) do not exceed 20 mrem/hr after 30 day irradiation and 1 day cooling. Taking into account all the current uncertainties, one can accept the proposed configuration as a baseline for further studies. It is interesting to note that the dose peaks are located about 2 m downstream of the collimators and of corresponding peaks in the beam loss distribution (Fig. 10), being a source of secondary particles irradiating the downstream quadrupoles. To provide adequate protection against low-energy neutrons at the hot spots, hydrogeneous liners (0.3 m thick concrete or polyethylene) inside and outside of the considered steel shielding will be needed. Analysis shows that such shielding is required in the first 30 meters of the utility section (Fig. 10) with somewhat reduced thickness or just with local shielding surrounding collimators in the rest of the section, especially while using the proposed scheme of the three fast bump-magnets (see Sect. 5).

Many engineering issues are related to this region design. The local shielding weight is about 12 ton/m. It occupies significant cross-sectional area and makes access to the region component a non-trivial task. Radiation levels inside it are extremely high preventing a hands-on maintenance, therefore the design should include the remotely operated crane to lift out the shielding and parts of the beam-line. The beam-line elements should be designed for fast remote maintenance. Remote operations are required for fine tuning of the collimator jaws. Another problem is the heat buildup in the collimation system. The power intercepted by COLL-1 and

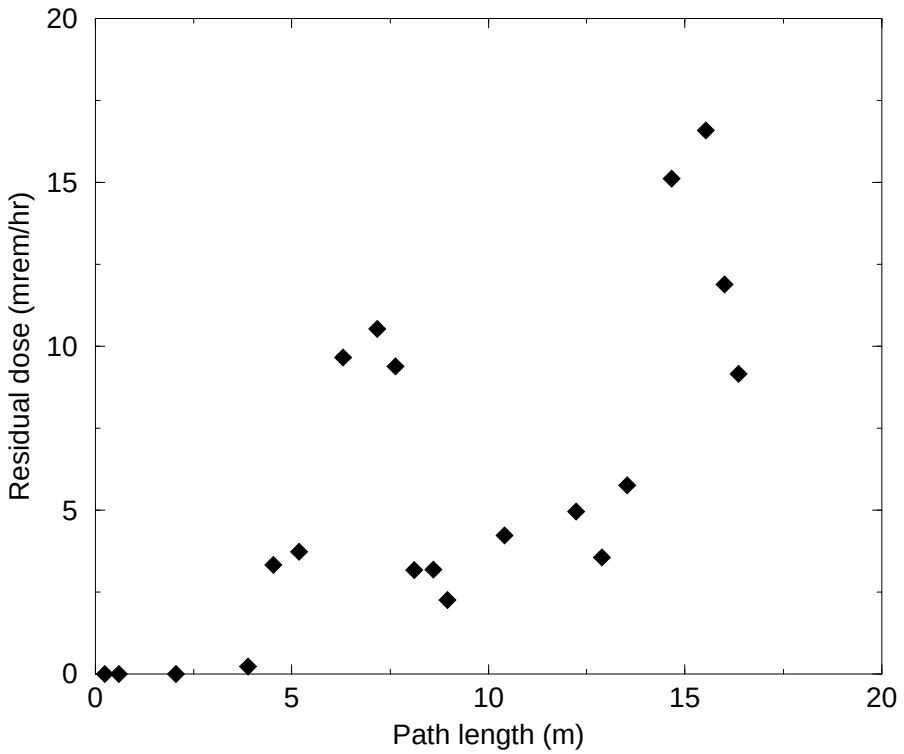

Figure 24: Residual dose rate on the outer shield surface in the collimation region.

COLL-2 is equal to about 3 and 4 kW, respectively. It is dissipated in the collimators themself and along 2-3 meters in the downstream beam-line. A corresponding cooling system should be able to remove this power. Radiation damage to the cables, cooling water pipes, beam diagnostics elements and other sensitive components is a serious issue in this region and will be considered for the entire machine in the near future.

9 Conclusions

Detailed energy deposition studies performed in the machine elements gave a possibility to deduce the tolerable beam loss in the Proton Driver. At the top energy in the arc for the considered lattice, the hands-on maintenance limits are 0.25 W/m in the open long beam pipes and 3 W/m in the magnets, while ground-water limit is 0.6 W/m.

A *3-stage collimation system* has been proposed based on detailed Monte-Carlo simulations at injection, acceleration, top energy and at RF capture. As a result of

thorough optimization, one concludes that the system consists of 1-mm thick tungsten primary collimators (scatterers) positioned at the horizontal and vertical edges of the beam after painting, followed by three secondary collimators with 0.5 mm offset with respect to the primary collimators and four supplementary collimators at 2.5 and 6.5 mm from the beam edge. Secondary and supplementary steel collimators are 0.3 m long and have a conical aperture according to the beam envelope after painting. In the considered preliminary lattice, such a system allows localization of more than 99% of beam loss in a special 60 m long utility section. Beam loss in the rest of the machine is on average 0.2 W/m. Replacement of the tungsten scatterers with short silicon bent crystals allows further improvement of the collimation performance, if beam loss at the top energy is less than a few percent of that at injection.

Radiation shielding design criteria are derived and the results of recent code benchmarking are presented justifying that one can reliably predict radiation fields at severe—from the calculation standpoint—conditions. Required thickness of the dirt shielding around the tunnel is driven by the worst case catastrophic *incredible* beam accident at 16 GeV and constitutes 26 feet or $\sim$8 meters. The work is underway at Fermilab towards the "worst credible accident" approach, which would allow to limit the amount of beam lost in such an accident to about 0.1% of that in the *incredible* case, resulting in the shield thickness reduced by about 10 feet. Local shielding found to provide necessary protection in the hottest 30-m part of the utility section consists of 2.3-m long and 0.5-m radius steel modules around the first secondary collimators, 0.4-m thick steel shielding at R=0.7 m at the first 16-m region and somewhat reduced in the rest of the utility section, with concrete or polyethylene liners at some locations.

Overall, despite of challenging parameters of the new Proton Driver proposed at Fermilab, beam loss and induced radiation effects can be controlled and reduced to the allowable levels. This work is based on a preliminary lattice design. Although the final lattice can be different, a majority of the results and main conclusions of this paper should remain valid. Directions of future work include: 1) sensitivity analysis (orbit errors, tune errors, collimator parameters and alignment etc.); 2) specified rates and parameters of beam halo interaction with collimators over the machine cycle; 3) radiation load to the cables, cooling system and beam diagnostics components and possible protective measures; 4) cooling water and air radioactivation; 5) further refinement of the machine, tunnel and beam loss calculation model at normal operation.

10 Acknowledgments

We express our gratitude to W. Chou for useful discussion and to V. Biryukov for his help with crystal collimation studies.

References

[1] S. Holmes, editor, "A Development Plan for the Fermilab Proton Source", Fermilab-TM-2021 (1997).

[2] W. Chou, "Proton Driver", *Proc. of the 7th ICFA Mini-Workshop on High-Intensity, High-Brightness Hadron Beams "Beam Halo and Scraping"*, September 13-15, 1999, Lake Como, Wisconsin.

[3] D. Ritson, "16 GeV Proton Driver Lattice", Private communication, March 2000.

[4] O. E. Krivosheev and N. V. Mokhov, "Tolerable Beam Losses and Shielding", *Proc. of the 7th ICFA Mini-Workshop on High-Intensity, High-Brightness Hadron Beams "Beam Halo and Scraping"*, September 13-15, 1999, Lake Como, Wisconsin.

[5] A. I. Drozhdin, C. J. Johnstone and N. V. Mokhov, "16 GeV Proton Driver Beam Collimation System", *Proc. of the 7th ICFA Mini-Workshop on High-Intensity, High-Brightness Hadron Beams "Beam Halo and Scraping"*, September 13-15, 1999, Lake Como, Wisconsin.

[6] I. S. Baishev, A. I. Drozhdin and N. V. Mokhov, "STRUCT Program User's Reference Manual", SSCL–MAN–0034 (1994); http://www-ap.fnal.gov/∼drozhdin/STRUCT/STR2.html.

[7] N. V. Mokhov, "The MARS Code System User Guide, Version 13(95)", Fermilab-FN-628 (1995); N. V. Mokhov et al., Fermilab-Conf-98/379 (1998); LANL Report LA-UR-98-5716 (1998); *nucl-th/9812038 v2 16 Dec 1998*; http://www-ap.fnal.gov/MARS/.

[8] N. V. Mokhov, "MARS Code Developments, Benchmarking and Applications", *Proc. of ICRS-9 International Conference on Radiation Shielding*, Tsukuba, Ibaraki, Japan, October 17-22, 1999, *Journal of Nuclear Science and Technology*, Suppl. 1, pp. 167-171 (March 2000), also Fermilab-Conf-00/066 (2000).

[9] A. I. Drozhdin and O. E. Krivosheev, "The Fermilab Proton Driver Beam Injection System Simulations", Fermilab–FN–694 (2000).

[10] "The NuMI Facility Technical Design Report", Fermilab (1998).

[11] A. I. Drozhdin, N. V. Mokhov et al., SSCL-Preprint-555 (1994).

[12] D. A. Edwards and M. J. Syphers, "An Introduction to the Physics of High Energy Accelerators", Wiley Series in Beam Physics and Accelerator Technology (1993).

[13] V. M. Biryukov, A. I. Drozhdin and N. V. Mokhov, "On Possible Use of Bent Crystal to Improve Tevatron Beam Scraping", *Proc. of the 1999 Particle Accelerator Conference*, New York, New York, March 29 - April 2, 1999, pp. 1234-1236; also Fermilab-Conf-99/072 (1999).

[14] V. M. Biryukov, "Crystal Channeling Simulation - CATCH 1.4 User's Guide", CERN SL/Note 93-74(AP) (1993).

[15] V. M. Biryukov, Yu. A. Chesnokov and V. I. Kotov, "Crystal Channeling and its Application at High Energy Accelerators", Berlin: Springer (1997).

[16] V. M. Biryukov, Private communication, IHEP (1999).

[17] C. T. Murphy, Private communication, Fermilab (1999).

[18] J. O. Johnson, Private communication, ORNL (2000).

[19] P. A. Aarnio *et al*, CERN TIS-RP/168 (1986) and CERN TIS-RP/190 (1987). A. Fassò *et al*, *Proc. IV Int. Conf. on Calorimetry in High Energy Physics*, La Biodola, Sept 20-25, 1993, Ed. A. Menzione and A. Scribano, World Scientific, p. 493 (1993). P. Aarnio and M. Huhtinen, *Proc. MC93, Int. Conf. on Monte Carlo Simulation in High Energy and Nuclear Physics*, p 1, ed. P. Dragowitsch, S. Linn and M. Burbank, World Scientific (1994). A. Fassò *at al, Proc. Specialists' Meeting on Shielding Aspects of Accelerators, Targets and Irradiation Facilities*, Arlington, Texas, April 28-29, 1994. NEA/OECD doc., p. 287 (1995).

[20] A. Fassø, A. Ferrari, J. Ranft, P.R. Sala, "New developments in FLUKA modelling hadronic and EM interactions", *Proc. 3rd Workshop on Simulating Accelerator Radiation Environments*, KEK, Tsukuba, Japan, 7-9 May 1997, Ed. H. Hirayama, KEK Proceedings 97-5, p. 32-43. A. Ferrari, and P.R. Sala, "The Physics of High Energy Reactions", *Proc. the Workshop on Nuclear Reaction Data and Nuclear Reactors Physics, Design and Safety*, International Centre for Theoretical Physics, Miramare-Trieste, Italy, 15 April-17 May 1996, edited by A. Gandini and G. Reffo, World Scientific, p. 424 (1998).

[21] http://mcnpx.lanl.gov.

[22] J. O. Johnson et al., "The Independent Verification and Validation of the ORNL SNS Linac Earth Berm Shielding Analysis", ORNL-SNS/TSR-177 (2000).

[23] M. Huhtinen and N. V. Mokhov, "A Cross-comparison of MARS and FLUKA Simulation Codes", CMS-Note (2000).

[24] G. Dugan, "Calculations of shielding requirements at 8 GeV for the Accelerator Division", Fermilab-02/13/1991; "Shielding criteria to define the 'red line' in Booster shielding assessments", Fermilab-02/14/1991.